Glass shard K-Ar dating of the Chalupas caldera major eruption: Main Pleistocene stratigraphic marker of the Ecuadorian volcanic arc

Mathilde Bablon, Xavier Quidelleur, Giuseppe Siani, Pablo Samaniego, Jean-Luc Le Pennec, Nouet Julius, Céline C. Liorzou, Santiago Santamaria, Silvana Hidalgo

Glass shard K-Ar dating of the Chalupas caldera major eruption: main Pleistocene stratigraphic marker of the Ecuadorian volcanic arc

Mathilde Bablon [a,b], Xavier Quidelleur [a], Giuseppe Siani [a], Pablo Samaniego [c,d], Jean-Luc Le Pennec [c,d], Julius Nouet [a], Céline Liorzou [e], Santiago Santamaría [a], Silvana Hidalgo [d]

[a] GEOPS, Université Paris-Sud, CNRS, Université Paris-Saclay, Rue du Belvédère, 91405 Orsay, France

[b] Université Côte d'Azur, CNRS, IRD, Observatoire de la Côte d'Azur, Géoazur, Sophia Antipolis 06560 Valbonne, France

[c] Laboratoire Magmas et Volcans, Université Clermont Auvergne, CNRS, IRD, OPGC, F-63000 Clermont-Ferrand, France

[d] Instituto Geofísico, Escuela Politécnica Nacional, Ladrón de Guevara E11-253, Ap. 2759, Quito, Ecuador

[e] Université de Bretagne Occidentale, Laboratoire Géosciences Océan, IUEM, 29280 Plouzané, France

Corresponding author: xavier.quidelleur@u-psud.fr (X. Quidelleur).

Keywords:

K-Ar dating; Glass shards; Ecuador; Chalupas; Ignimbrite eruption.

WORD COUNTS:

Abstract: 249
Text: 4440
Reference number: 81
Figures: 5
Tables: 4
Appendix: 1

Additional information:

- Declarations of interest: none
- Funding: INSU CNRS TelluS Aleas ([INSU 2015-ALEAS], [INSU 2016-ALEAS]) and LMI IRD ([2012-16 LMI SVAN-IRD]) programs for field trips, sampling, preparations of samples, K and Ar measurements for ages, as well as ICP-AES and electron microprobe analyses for major and trace elements.
- All figures should be 2 columns-wide. They will be in color only for the web version, and in black and white for the printed version.

Abstract

New K-Ar ages obtained on juvenile pumice glass shards indicate that the Chalupas ignimbrite, one of the main Pleistocene tephra markers of the Ecuadorian arc, was emplaced at 216 ± 5 ka. Morphology and major and trace element contents of the glass shards are similar to those of ash layers from deep-sea cores and allow correlation between continental deposits and marine tephra layers. Based on biostratigraphy and $\delta^{18}O$ data, the age models of these cores support our K-Ar age. Fine ashes from the Chalupas eruption column have been found about 1000 km away from the source caldera, and the estimated deposit volume of both ignimbrite and co-ignimbrite deposits ranges from 200 to 265 km^3. This suggests that the Chalupas event could have been strong enough to reach the stratosphere and inject large amount of SO_2 in both hemispheres, possibly impacting global temperatures. In addition, the age of the Chalupas ignimbrite obtained here could provide a new radiometric constraint for the age of isotope stage 7 recorded in orbitally-tuned $\delta^{18}O$ deep-sea cores. This study highlights the relevance of K-Ar dating applied to small glass shards from massive ignimbrite deposits, and the potential that it represents to improve risk assessments in volcanic zones where dating crystals is not possible. Finally, detailed tephrochronology of deep-sea cores and correlation between marine ash-layers and continental volcanic deposits constitute a strong tool to investigate the eruptive history of an active volcanic arc whose proximal products have been eroded or deeply buried by younger deposit sequences.

1. Introduction

Major explosive caldera-forming eruptions are colossal volcanic phenomenon that can eject large volumes of tephra and volatiles into the atmosphere and spread tephra over wide areas. Such events can impact the local population, infrastructures and natural environment, namely the climate system at regional and even global scales (e.g. McCormick et al., 1995; Robock, 2000; Cole-Dai, 2010). Tephrochronology is a powerful tool for dating and correlating deposit sequences scattered over large areas. The method consists in comparing tephra features, such as their age or position in the stratigraphic column, their chemical and mineralogical composition, as well as glass shard morphology, in order to match the deposits associated with a single volcanic event (e.g., Lowe, 2011). Consequently, tephrochronology allows us to investigate magmatic processes, recurrence and impact of past major eruptions, and hence better define the volcanic hazards and its frequency-magnitude relationships. As the time period between tephra emission and deposit is mostly on the order of hours or days (Robock, 2000; Mills, 2000; Rose and Durant, 2009), dating tephra fallouts is a robust way to determine the age of the corresponding eruption. The $^{40}Ar/^{39}Ar$ single grain dating method applied on K-rich minerals, such as sanidine, biotite and even plagioclase crystals, is commonly used to date tephra older than ~50 ka, i.e. for which ^{14}C age determination is not possible. For instance, this technique has been used to accurately date the Young Toba Tuff and investigate the relationship between this major eruptive event and global cooling (e.g., Williams et al, 2009; Storey et al., 2012; Mark et al., 2014), or to date the Yellowstone Tuffs and study the eruptive history of the caldera (e.g., Ellis et al., 2012; Matthews et al., 2015). In offshore Central America this method was used to study characteristics, output rates and recurrence of explosive eruptions (Schindlbeck et al., 2016a; b). Also, applications to North

Atlantic marine cores have helped to refine the age of ice-rafted debris recorded in offshore Iceland (Lacasse and van den Bogaard, 2002).

As crystals may not be systematically present in pumice samples, glass may be the only juvenile material that can be dated. While the $^{40}Ar/^{39}Ar$ technique is not always suitable for glass shard dating because of ^{39}Ar recoil occurring during irradiation for non-crystalline phases and small grains with high surface area to volume ratio (e.g., McDougall and Harrison, 1999; Morgan et al., 2009), the potassium-argon (K-Ar) technique may be successfully employed (e.g., Milne, 1973; Pinti et al., 2001). In this paper, we focus on the Chalupas ignimbrite, one of the main Pleistocene stratigraphic markers in Ecuador, and we present new K-Ar ages carried out on pumice glass shards and biotite crystals. We also compare the morphology and geochemistry of glass shards of pumices with those of distal tephra fallouts from Ocean Drilling Project's (ODP) Pacific deep-sea cores in order to provide support for our K-Ar age determination and investigate the volume and magnitude of this major eruption.

2. Quaternary stratigraphic markers of the Ecuadorian arc

In Ecuador, at least three large caldera systems originate from past Quaternary volcanic activities. In the northern part of the current Ecuadorian arc, the ~10 km-wide *Chalpatán* caldera is located within the Interandean Valley, near the border between Ecuador and Colombia (Fig. 1B). This poorly documented caldera could have collapsed after a powerful eruption that occurred during the Quaternary (Barberi et al., 1988). Further south, Chalupas and Chacana (Fig. 1B) are the widest caldera systems in Ecuador. The *Chacana* volcanic system is located in the Eastern Cordillera, about 30 km from Quito, the capital city of Ecuador. It experienced two large plinian eruptions at ~160-190 ka (Bigazzi et al., 1992; Hall and Mothes, 1997; Hall and Mothes, 2008c), whose deposits, the Pifo fall layers, constitute one of the main Pleistocene stratigraphic markers of the northern part of the

Ecuadorian arc (e.g., Robin et al., 2009; Alvarado et al., 2014; Bablon et al., 2019b). About 50 km south of Chacana, *Chalupas* caldera results from a major Pleistocene ignimbrite eruption. In this study, we focus on the latter as only an unpublished $^{40}Ar/^{39}Ar$ date is available for the Chalupas ignimbrite (Hammersley, 2003; Beate et al., 2006; Mothes and Hall, 2008).

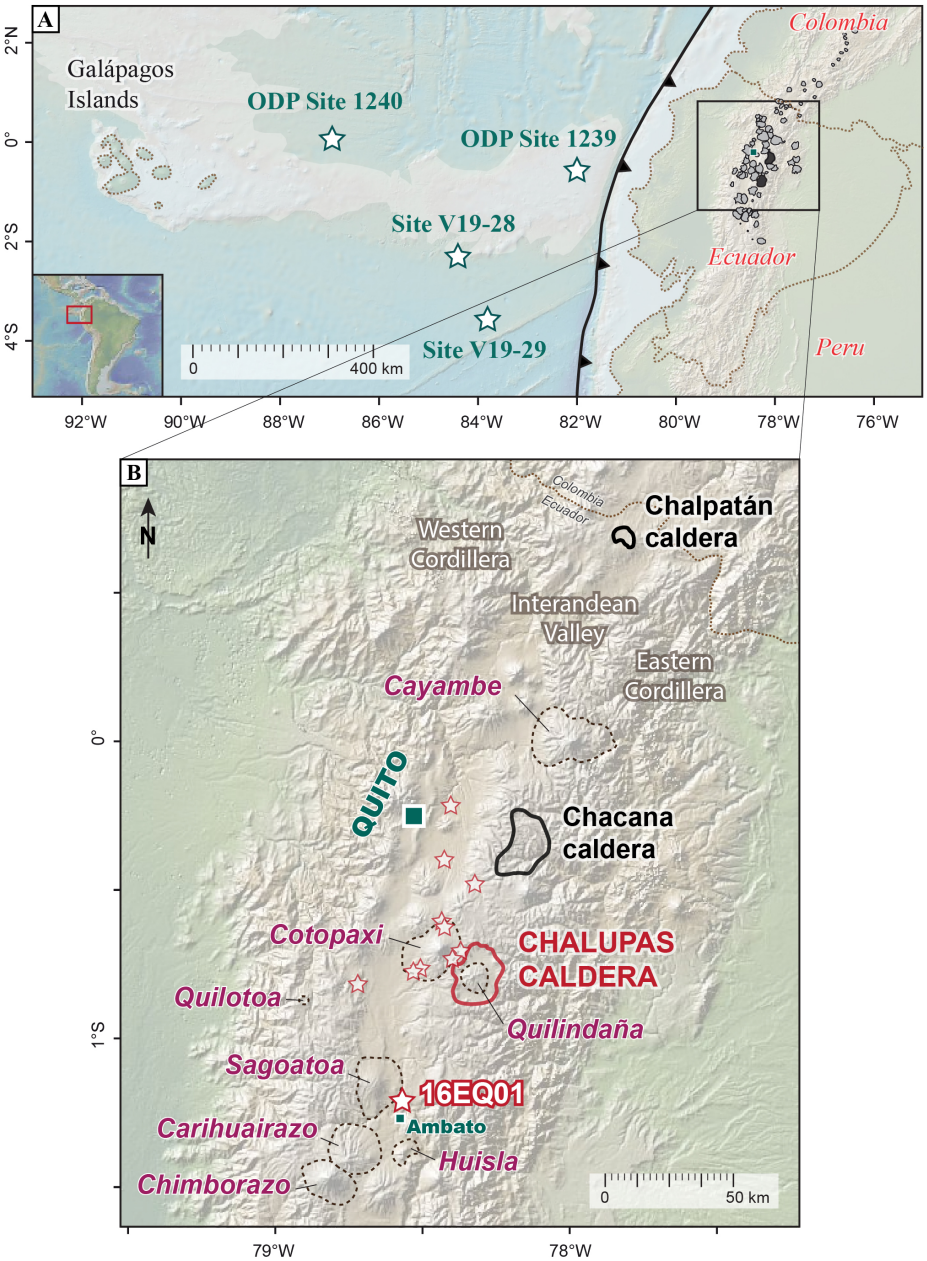

Fig. 1. Location of the samples presented in this study. A) Map of Ecuador and the Galápagos Islands. Grey circles represent Quaternary volcanoes of Ecuador and Colombia. Stars represent the location of ODP and Ninkovich and Shackleton (1975) drilling sites presented in the text. B) Zoom on the central part of the volcanic arc, showing volcanoes and calderas mentioned in the text. The Chalupas caldera is represented in red, and the location of the Chalupas ignimbrite sample (16EQ01) with a big white and red star. Small white and red stars indicate the location of Chalupas ignimbrite samples whose major and trace element content are provided in Appendix A. Dashed lines are basal contours of volcanoes, while continuous lines are used for calderas.

Because of its large-scale dispersion, as well as its rather unique rhyolite composition and easily recognizable facies, the Chalupas ignimbrite deposits constitute an important stratigraphic marker of the southern and central parts of the Ecuadorian volcanic arc in the Late Pleistocene record. Thereby, it is important to precisely date this event, in order to provide a geochronological constraint to the construction of Ecuadorian volcanoes, as well as to the Late Pleistocene deformation of the volcanic and volcano-clastic deposits located within the Interandean Valley (e.g., Alvarado et al., 2014). In addition, dating events associated to such major eruptions allow us to investigate their recurrence through time and improve hazard assessment in this populated area of the Andes, and may allow correlation with climatic records to infer any possible global effect of these eruptions.

3. The Chalupas ignimbrite

The Chalupas volcanic complex (Lat. 00°47'S; Long. 78°18'W) is located in the Eastern Cordillera of Ecuador, about 50 km from Quito (Fig. 1B), to the west-southwest of Cotopaxi volcano. This volcanic system is characterized by a conspicuous 16 k-wide and 18 km-long caldera (Mothes and Hall, 2008; Bernard and Andrade, 2011) that was formed during a large ignimbrite eruption of rhyolitic composition. Andesite to dacite lava flows crop out southwest of the caldera and are the main remnants of the pre-caldera volcanic system (Barberi et al., 1988; Beate et al., 2006). Afterwards, Quilindaña andesitic stratovolcano grew in the center of the caldera (Córdova et al, 2018; Fig. 1B). Channelized by relief and volcanoes already present during the eruption, the Chalupas ignimbrite was deposited in the Interandine Valley south of Quito. Within a radius of about fifty kilometers, the proximal deposits of the Chalupas ignimbrite are a few tens of meters thick (e.g., Beate et al., 2006; Hall and Mothes, 2008a; 2008b; Ordóñez, 2012; this study). They consist of a non-welded juvenile pyroclastic material made up of poorly sorted pumiceous blocks in an ash-rich

matrix. Pumices contain rare biotite and plagioclase crystals, as well as accessory apatite and Fe-Ti oxides. Onshore tephra fallout deposits associated to this event spread out to the west and crop out as far as the coast, ~300 km from the caldera (Jackson et al., 2019).

Beate et al. (2006) reported an unpublished $^{40}Ar/^{39}Ar$ age of 211 ± 14 ka for the Chalupas ignimbrite, obtained on plagioclase crystals (Hammersley, 2003). Although this age is in agreement with stratigraphic relationships that have been described between the Chalupas ignimbrite and deposits from Cotopaxi (Hall and Mothes, 2008a), Huisla (Ordóñez, 2012; Espín, 2014), Sagoatoa (Bablon et al., 2019a), Quilotoa (Hall and Mothes, 2008b), Carihuairazo (Ordóñez, 2012), and Chimborazo (Bernard et al., 2008; Samaniego et al., 2012) volcanoes (Fig. 1B), it is not supported by any description of data, the standards used, age spectra, nor the inverse isochron.

4. Materials and methods

4.1. Sampling and preparation of samples for K-Ar dating

The Chalupas ignimbrite deposit was sampled towards the base of a ~30 m-high quarry outcrop, in the vicinity of Ambato city, 55 km southwest of the caldera (sample 16EQ01; Fig. 1B).

The pumice blocks were crushed manually in an agate mortar, sieved and ultrasonically rinsed with deionized water. A magnetic separator was used to remove the andesite xenoliths, and grains were separated using heavy liquids within a narrow density range (see below). Such procedure allows the preservation of the massive structure of the glass shards and minerals.

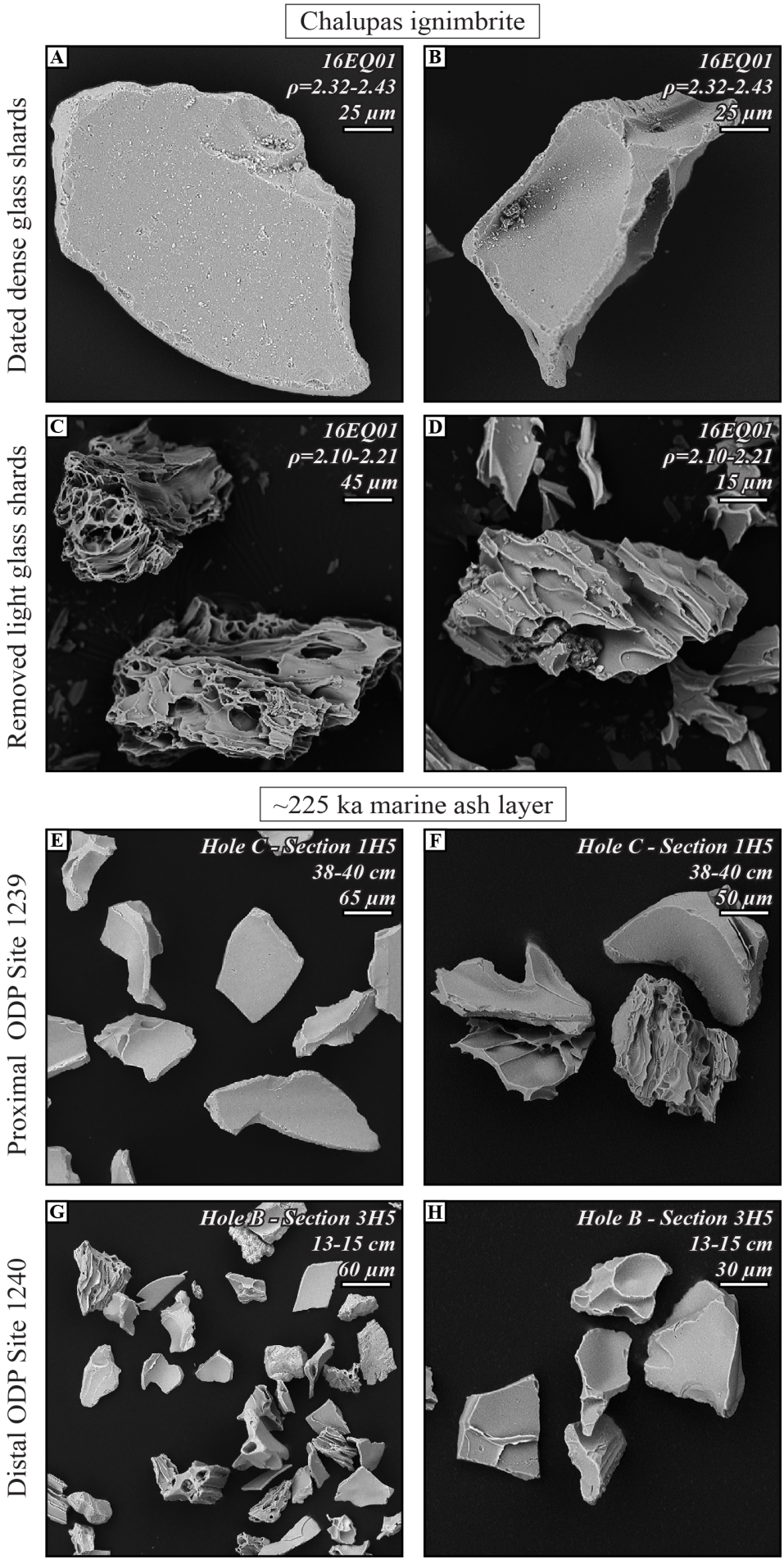
Chalupas ignimbrite
Dated dense glass shards
Removed light glass shards
~225 ka marine ash layer
Proximal ODP Site 1239
Distal ODP Site 1240
A
16EQ01
ρ=2.32-2.43
25 µm
B
16EQ01
ρ=2.32-2.43
25 µm
C
16EQ01
ρ=2.10-2.21
45 µm
D
16EQ01
ρ=2.10-2.21
15 µm
E
Hole C - Section 1H5
38-40 cm
65 µm
F
Hole C - Section 1H5
38-40 cm
50 µm
G
Hole B - Section 3H5
13-15 cm
60 µm
H
Hole B - Section 3H5
13-15 cm
30 µm

166

Fig. 2. Scanning Electron Microscopy (SEM) images of glass shards. A-B) Dense, blocky glass shards of the dated fraction of continental Chalupas ignimbrite. C-D) Light glass grain fragments of Chalupas ignimbrite, with a lower density due to a significant increase of vesicle content. E-F) Glass shards from the proximal ODP Site 1239, deposited at ~225 ka. G-H) Glass shards from the distal ODP Site 1240, deposited at ~225 ka.

The morphology of the glass shards, studied using a Scanning Electron Microscope (SEM), shows a clear difference between the dense glass shards, massive and rather smooth (Figs. 2A and B), and which were used for dating, and the light glass shards, significantly stringier and more vesicular (Figs. 2C and D). Note that glass shards (80-125 µm; ρ=2.32-2.43) selected from the Chalupas ignimbrite represent less than 5 vol.% of the initial sample. In addition, biotite crystals (>125 µm; ρ=2.85-3.28) were also separated for dating.

Age measurements were performed using the unspiked K-Ar Cassignol-Gillot technique (Gillot et al., 2006) in the GEOPS laboratory at Orsay (Paris-Sud University, France). This technique is suitable for dating groundmass of young lava flows, as well as K-feldspars from explosive deposits, and has been successfully applied for studying Quaternary subduction volcanic products from many places, such as Ecuador (Bablon et al., 2018; 2019a), Argentina or Lesser Antilles (e.g., Samper et al., 2009; Germa et al., 2010; 2011; Ricci et al., 2015). Comparison with the age of the Matuyama-Brunhes paleomagnetic field reversal has shown that it can also be used to date glass shards from volcanic tephra (Pinti et al., 2001). However, this technique requires fresh glass shards, as both the amorphous nature of glass and the large surface to volume ratio of the grains favor a high mobility of K and/or Ar (Cerling et al., 1985). It seems that the K-Ar method is most successful in dating volcanic glass, since a significant recoil effect, induced by the sample irradiation, biases $^{40}Ar/^{39}Ar$ ages of glass shards toward erroneous older values (McDougall and Harrison, 1999; Morgan et al., 2009). The full description of analytical procedures, standards and uncertainty calculation is given in Bablon et al. (2018). Ages have been calculated using decay constants of Steiger and Jäger (1977). The ^{40}Ar signal calibration was performed using an age of 24.21 Ma for HD-B1 biotite standard (Hess and Lippolt, 1994). Age results are given in Table 1 at the 1-σ

confidence level. Each argon measurement has been carried out on ~0.9 and ~0.5 g of glass shards and biotite crystals, respectively.

4.2. Tephra layers in deep-sea cores

For this study, we selected two deep-sea cores from Leg 202 ODP Site 1239, located near the Ecuadorian margin, and ODP Site 1240, located closer to the Galápagos Islands (Fig. 1A; Shipboard Scientific Party, 2003). These cores present many marine ash layers visible to the naked eye throughout the sedimentary sequence, 24 for the proximal ODP Site 1239 and 8 for the distal ODP Site 1240, covering the last ~15 and ~2.3 Ma, respectively (Shipboard Scientific Party, 2003). To investigate the correlation between these marine deposits and the proximal deposits of the Chalupas eruption, we focused on ash layers younger than 300 ka. One layer is significantly thicker than the others, and reaches ~16 cm-thick in Site 1239, and ~3 cm-thick in Site 1240. Within cores from Site 1239, the ash layer is located between 6.65 and 6.83 mcd (meters composite depth), between 6.87 and 7.07 mcd, and between 6.72 and 6.88 mcd, for holes A, B and C, respectively. Within cores from Site 1240, the ash layer is located between 25.69 and 25.71 mcd, and between 25.69 and 25.72 mcd, for holes B and C, respectively (Shipboard Scientific Party, 2003). It is composed of millimetric glass shards with some calcareous nannofossils, foraminifera and diatoms (mainly *Gephyrocapsa spp.*, *Globorotalia menardii* and *Neogloboquadrina dutertrei*; Shipboard Scientific Party, 2003), the proportion of which significantly decreases in the central part of the layer. For each ash layer from both Sites 1239 and 1240, we collected three to six 2 cm-thick samples every 5 cm depth of the core section. Sample preparation for electron microprobe analyses consisted in removing clay by washing and manually sieving each sample at 63 or 40 µm for proximal (Site 1239) and distal (Site 1240) cores,

218 respectively. Then, glass shards were individually selected by hand under a magnifier and
219 mounted on epoxy resin beads before polishing.
220
221 *4.3. Geochemical analyses*

222 Whole-rock major and trace element content of the continental Chalupas ignimbrite
223 sample and trace element content of marine tephra samples were measured by ICP-AES
224 (Inductively Coupled Plasma - Atomic Emission Spectrometry) at the Laboratoire
225 Géosciences Océan of the Université de Bretagne Occidentale (Brest, France), following the
226 procedure detailed in Cotten et al. (1995). Relative uncertainties are ≤ 2% for major elements
227 and ≤ 5% for trace elements.
228 Major element measurements of single glass shards were performed on CAMECA
229 SX-100 and SX-FIVE electron microprobes at the University Pierre and Marie Curie
230 (CAMPARIS, France). Relative uncertainties are < 0.6% for SiO_2; ~1% for Al_2O_3, < 3% for
231 CaO and MgO, < 4% for Na_2O, < 5% for Fe_2O_3, < 6% for K_2O, 10% for TiO_2 and ~30% for
232 MnO.
233

234 **5. Results**

235 *5.1. K-Ar age of Chalupas ignimbrite*

236 K-Ar measurements have been performed on dense glass shards (Figs. 2A and B) and
237 biotite crystals from continental Chalupas ignimbrite. Dated dense glass shards have a fresher
238 aspect and a more massive structure than lighter and vesiculated shards (Figs. 2C and D) that
239 have been removed using heavy liquids. In fact, as vesicles contain gases, they are prone to a
240 high contamination in atmospheric argon, and the content of radiogenic argon is thus more
241 difficult to determine precisely.

The potassium content of glass shard samples is 3.54 ± 0.04 %, and reaches 6.66 ± 0.07 % for biotite crystals (Table 1). The content of radiogenic argon, which derives from the radioactive decay of ^{40}K, ranges between 5.1 and 12.3 ± 0.10 %. From these values combined with the ^{40}K decay constants (Steiger and Jäger, 1977), we obtain ages of 216 ± 5 and 286 ± 5 ka for the glass shards and biotite crystals from the Chalupas ignimbrite, respectively (Table 1).

Table 1
K-Ar data obtained in this study. Column headings indicate sample name, coordinates (Universal Transverse Mercator coordinate system, WGS84 spheroid, Zone 17), dated material, potassium concentration in percent, radiogenic argon content in percent and 10^{11} atoms per gram, ages and weighted mean age in ka (1-σ uncertainty).

Sample	Longitude (m)	Latitude (m)	Phase	K (%)	$^{40}Ar^{*}$ (%)	$^{40}Ar^{*}$ x 10^{11} (at/g)	Age ± 1σ (ka)	Mean age (ka)
Chalupas ignimbrite								
16EQ01	769765	9867875	Glass shards	3.54 ± 0.04	5.16 ± 0.10	7.856 ± 0.155	213 ± 5	**216 ± 5**
					5.18 ± 0.10	8.009 ± 0.158	217 ± 5	
					5.09 ± 0.10	8.063 ± 0.152	218 ± 5	
			Biotite crystals	6.66 ± 0.07	12.26 ± 0.10	19.740 ± 0.161	284 ± 5	**286 ± 5**
					7.14 ± 0.10	20.091 ± 0.282	289 ± 6	

5.2. Geochemical analyses

Results of whole-rock major and trace element contents of continental Chalupas ignimbrite are provided in Table 2. Analyses show that the chemical composition of the Chalupas ignimbrite is highly homogeneous at the deposit scale (Table 2; Appendix A).

Table 2
Whole-rock major and trace element composition of our Chalupas ignimbrite sample (16EQ01), with mean and standard deviation of analyses performed on 20 different outcrops of the Chalupas ignimbrite across Ecuador (Appendix A; Barberi et al., 1988; Bryant et al., 2003; Ancellin et al., 2017; Córdova, 2018), measured by ICP-AES. All analyses of major elements were brought down to a total of 100% on a water-free basis.

Whole-rock Chalupas ignimbrite					
Major elements (wt.%)			Trace elements (ppm)		
	16EQ01	*Other outcrops*		16EQ01	*Other outcrops*
SiO_2	74.72	*74.64 ± 0.49*	Sc	2.06	*2.06 ± 0.23*
TiO_2	0.24	*0.25 ± 0.02*	V	13.46	*13.32 ± 3.76*
Al_2O_3	13.77	*13.89 ± 0.24*	Cr	<<	*3.65± 2.02*
Fe_2O_3	1.46	*1.42 ± 0.18*	Co	0.32	*3.00 ± 2.18*
CaO	1.22	*1.25 ± 0.08*	Ni	<<	*2.07 ± 1.12*
MgO	0.34	*0.33 ± 0.03*	Rb	191.42	*172.76 ± 5.58*
MnO	0.05	*0.05 ± 0.00*	Sr	201.14	*207.94 ± 6.50*
K_2O	4.29	*4.38 ± 0.23*	Y	12.41	*13.22 ± 1.92*
Na_2O	3.87	*3.74 ± 0.29*	Zr	153.25	*162.35 ± 13.49*
P_2O_5	0.04	*0.04 ± 0.01*	Nb	10.12	*11.29 ± 0.36*
L.O.I.	3.47		Ba	1099.24	*1059.00 ± 49.29*
			La	30.9	*31.05 ± 1.11*
			Ce	55.08	*56.49 ± 2.52*
			Nd	19.88	*19.50 ± 4.32*
			Sm	3.37	*3.58 ± 0.19*
			Eu	0.42	*0.60 ± 0.04*
			Gd	2.82	*2.67± 0.29*
			Dy	2.07	*2.07 ± 0.14*
			Er	1.09	*1.26 ± 0.07*
			Yb	1.24	*1.25 ± 0.08*
			Th	21.7	*21.95 ± 1.33*

Major element content of the dated continental sample of the Chalupas ignimbrite and marine tephra layers, determined using electron microprobe on single glass shards, are given in Table 4.

Table 3
Major element contents of single glass shards measured by electron microprobe. All analyses were recalculated to a total of 100%. We report only analysis with oxide sum above 93%. Std: standard deviation.

274

Leg ODP 202 - Site 1239 - Hole C - Section 1H5 - 43-45 cm

wt.%																	*Mean*	*Std*
SiO_2	78.96	77.27	77.47	76.27	76.61	75.42	76.50	76.28	76.00	76.66	77.08	76.59	75.44	76.11	77.92	76.31	**76.68**	0.90
TiO_2	0.27	0.29	0.09	0.19	0.33	0.38	0.21	0.10	0.12	0.20	0.07	0.12	0.22	0.19	0.18	0.09	**0.19**	0.09
Al_2O	13.49	14.31	14.44	14.08	14.28	13.76	13.26	13.80	14.00	14.22	14.17	13.81	14.20	13.73	13.67	13.88	**13.94**	0.32
Fe_2O	0.81	1.13	1.10	1.06	0.91	0.98	1.10	0.60	0.68	0.63	0.53	0.90	1.08	1.22	1.27	0.71	**0.92**	0.24
CaO	1.22	1.00	1.14	1.15	1.00	0.91	1.09	0.81	0.82	0.84	0.69	0.86	1.22	1.19	1.15	0.71	**0.99**	0.19
MgO	0.20	0.22	0.19	0.16	0.26	0.23	0.23	0.10	0.14	0.13	0.14	0.06	0.29	0.25	0.27	0.11	**0.19**	0.07
MnO	-0.01	0.01	0.10	0.03	0.03	0.08	0.02	0.03	0.04	0.08	0.21	0.13	0.07	-0.01	0.03	-0.03	**0.05**	0.06
K_2O	3.30	3.87	3.70	4.58	3.86	5.09	4.54	4.98	4.88	4.21	3.97	4.28	4.05	3.86	3.69	5.27	**4.26**	0.57
Na_2O	1.77	1.90	1.78	2.48	2.72	3.16	3.06	3.29	3.32	3.03	3.14	3.25	3.42	3.46	1.81	2.95	**2.78**	0.63

Leg ODP 202 - Site 1240 - Hole C - Section 3H2 - 128-130 cm

wt.%														*Mean*	*Std*
SiO_2	76.88	76.02	77.75	75.96	75.85	76.71	75.87	75.80	75.00	77.36	76.17	75.53	76.38	**76.25**	0.76
TiO_2	0.14	0.23	0.17	0.11	0.25	0.17	0.20	0.22	0.21	0.13	0.11	0.20	0.23	**0.18**	0.05
Al_2O	13.94	13.53	12.77	13.30	14.03	13.83	14.24	14.15	14.48	13.85	14.08	13.67	13.87	**13.83**	0.44
Fe_2O	0.94	1.31	0.96	1.16	1.25	1.00	1.08	1.06	1.25	0.91	1.01	1.07	1.04	**1.08**	0.13
CaO	0.95	1.05	1.02	0.95	1.15	0.82	1.02	1.13	0.81	1.14	1.00	1.24	0.98	**1.02**	0.13
MgO	0.19	0.24	0.18	0.19	0.24	0.18	0.23	0.18	0.26	0.26	0.20	0.24	0.17	**0.21**	0.03
MnO	0.13	0.07	0.02	0.22	-0.05	0.03	0.07	0.03	0.06	-0.03	-0.08	0.03	0.11	**0.05**	0.08
K_2O	3.71	4.63	4.53	4.73	4.12	4.79	4.60	4.20	4.77	3.54	4.20	4.52	4.76	**4.39**	0.41
Na_2O	3.12	2.91	2.59	3.38	3.17	2.49	2.70	3.23	3.16	2.83	3.32	3.51	2.45	**2.99**	0.35

Chalupas ignimbrite (16EQ01)

wt.%													*Mean*	*Std*
SiO_2	75.45	75.50	75.90	74.37	75.44	75.21	74.51	75.94	75.29	75.10	76.10	74.37	**75.27**	0.59
TiO_2	0.26	0.16	0.21	0.37	0.24	0.23	0.24	0.19	0.35	0.25	0.21	0.25	**0.25**	0.06
Al_2O	14.32	13.72	14.11	13.83	14.65	14.31	14.89	13.93	14.53	13.76	14.36	14.12	**14.21**	0.37
Fe_2O	1.18	0.54	0.75	1.06	0.39	0.99	0.63	0.97	0.94	0.93	0.54	1.41	**0.86**	0.30
CaO	1.03	1.03	1.04	1.14	0.96	1.03	0.98	1.10	1.06	1.04	1.05	1.15	**1.05**	0.06
MgO	0.17	0.16	0.22	0.24	0.08	0.22	0.13	0.17	0.22	0.22	0.18	0.22	**0.19**	0.05
MnO	0.08	0.02	0.05	0.08	0.07	0.12	0.02	0.02	0.10	0.05	0.05	0.05	**0.06**	0.03
K_2O	4.39	4.58	4.19	4.36	4.58	4.51	4.49	4.24	4.43	4.36	4.37	4.51	**4.42**	0.12
Na_2O	3.11	4.30	3.53	4.55	3.59	3.38	4.10	3.44	3.09	4.28	3.13	3.92	**3.70**	0.51

275

276 **Table 4**
277 Trace element composition of the bottom and the top parts of marine tephra layers from ODP 1239 and 1240
278 Sites, measured by ICP-AES.

279

ODP tephra layers				
Trace elements (ppm)	Site 1239 - Hole B - Section 1H5		Site 1240 - Hole B - Section 3H5	
	93-95 cm (top of the layer)	98-100 cm (bottom of the layer)	5-7 cm (top of the layer)	13-15 cm (bottom of the layer)
Sc	2.40	2.23	2.47	2.65
V	16.09	16.78	31.21	22.21
Cr	4.95	10.36	13.79	10.04
Co	1.44	2.30	1.61	1.75
Ni	6.01	6.49	17.13	10.42
Rb	146.04	126.99	88.04	152.24
Sr	196.15	192.95	298.73	226.68
Y	11.45	10.86	11.98	11.76
Zr	138.58	127.32	120.63	141.74
Nb	9.95	8.95	7.14	9.30
Ba	989.84	876.87	927.54	993.81
La	21.04	20.63	24.28	24.02
Ce	46.58	43.54	41.78	45.16
Nd	14.71	15.56	16.30	17.01
Sm	3.10	2.71	4.19	2.89
Eu	0.61	0.60	0.46	0.60
Gd	2.06	1.97	2.35	2.43
Dy	1.59	1.67	1.62	1.73
Er	1.28	1.22	1.68	1.09
Yb	1.08	1.01	1.18	1.16
Th	18.08	17.88	15.78	18.31

Overall, marine tephra from proximal and distal ODP cores (light and dark blue respectively; Figs. 3A and B), and the continental Chalupas ignimbrite (grey circles and squares; Figs. 3A and B), display a rather homogeneous rhyolitic composition, with SiO_2 and K_2O contents higher than 74.3% and 3.3%, respectively. They belong to the high-K calc-alkaline magmatic suite (orange field; Fig. 4A), which characterizes products from the Eastern Cordillera in Ecuador. Whole-rock measurements of minor and trace element contents show that the Chalupas ignimbrite and the proximal and distal marine tephra layers are homogeneous and enriched in most incompatible elements (e.g., Rb, Ba, Th, K) and depleted in Nb, Sr and Ti (Fig. 3D), typical of subduction-related volcanic products.

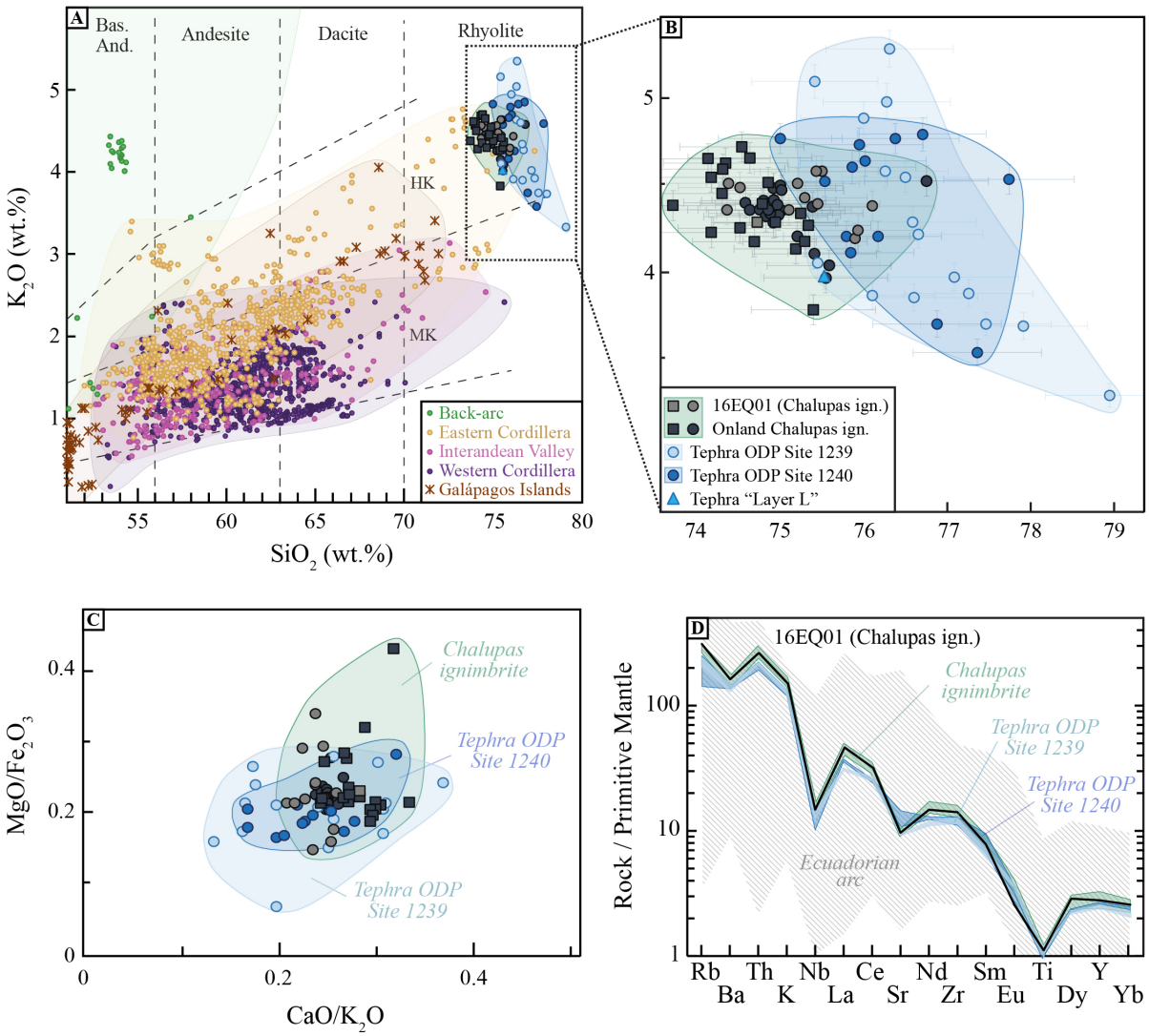

Fig. 3. A) K_2O vs SiO_2 diagram with composition fields of all whole-rock data obtained for the Ecuadorian arc (purple, pink, yellow and green for the Western Cordillera, Interandean Valley, Eastern Cordillera and back-arc, respectively) and the Galápagos Islands (brown stars; Georoc database). HK, MK: high-K and medium-K calc-alkaline series. B) Detail on composition of rhyolite pumices studied in this work. Squares: Whole-rock measurements (Table 2; Appendix A; Barberi et al., 1988; Bryant et al., 2006; Ancellin et al., 2017; Córdova, 2018). Circles: measurements of single glass shards (Table 3; Jackson et al., 2019). Triangle: ~220 ka "Layer L" from deep-sea cores (Ninkovich and Shackleton, 1975; see below). Blue field represents compositions that we associate to a single event of Chalupas ignimbrite. C) MgO/Fe_2O_3 ratio as a function of CaO/K_2O ratio. Legend as in Fig 3B. Error bars are included in the size of the symbols. D) Incompatible elements normalized to primitive mantle spider diagram (Sun and McDonough, 1989) of continental sample 16EQ01 (Chalupas ignimbrite; Table 2) and ODP marine tephra (Table 4). Purple and hatched grey domains represent the range of all values obtained for the Chalupas ignimbrite (Appendix A) and the Quaternary Ecuadorian arc (Georoc database).

6. Discussion

6.1. Use of K-Ar dating method for determining the age of Quaternary pumice deposits

Glass shards from the Chalupas ignimbrite have a significantly younger age than biotite crystals (216 ± 5 and 286 ± 5 ka, respectively; Table 1). Glass shards are fragments of the juvenile fraction that solidified during the eruption, whereas the biotite phenocrysts could crystallize earlier in the magmatic reservoir. The older age of biotite crystals could therefore be explained by the presence of inherited radiogenic argon and/or excess argon trapped in the differentiated magma, where partial pressure of argon prior eruption is high and not equilibrated with atmosphere (e.g., Morgan et al., 2009; Hora et al., 2010). Alternatively, the potassium leaching favored by the lamellar structure of biotite crystals may also result in older ages. However, we note that the K content of Chalupas biotite phenocrysts (6.7%; Table 1) is similar to the mean values of 6.9% obtained for biotite crystals contained in rhyolite products from worldwide arc volcanoes (1562 measurements; Georoc database) and 6.8% obtained for dacite and rhyolite Ecuadorian pumices (61 measurements from Monzier et al., 1999; Samaniego et al., 2005; Garrison et al., 2011; Chiaradia et al., 2014; Bernard et al., 2014; Béguelin et al., 2015), which suggests that our biotite crystals are rather fresh. As both phenomena (i.e., inherited and/or excess argon and leaching) may induce older ages for biotite crystals, we propose that the age of the event associated with the eruption of the Chalupas ignimbrite is 216 ± 5 ka, as obtained from glass shards. The very small amount of plagioclase phenocrysts present in the sample prevented us from using this mineral phase for dating. However, our age obtained on glass shards refines and agrees with the unpublished $^{40}Ar/^{39}Ar$ age of 211 ± 14 ka obtained from plagioclase crystals (Beate et al., 2006).

6.2. Age of marine tephra and correlation with the Chalupas eruption

The occurrence of widespread volcanic ash layers in deep-sea sediments is related to the transport in the atmosphere to the ocean of glass shards, which rapidly descend the water

column and reach the seafloor in a few days (e.g., Wiesner et al., 1995; Carey, 1997; Manville and Wilson, 2004; Wetzel, 2009), i.e. instantaneously with respect to geological time-scales.

The stratigraphic age of the analyzed rhyolitic tephra occurring within both ODP 1239 and 1240 Sites can be inferred using the oxygen isotope record ($\delta^{18}O$) from these deep-sea cores previously published by Rincón-Martínez et al. (2010), Dyez et al. (2016), and Rippert et al. (2017), respectively. The age model of $\delta^{18}O$ records was based on the global $\delta^{18}O$ stack of Lisiecki and Raymo (2005), through $\delta^{18}O$ measurements on the benthic foraminifera *Cibicidoides wuellestorfii* and on the planktonic foraminifera *Globorotaloides hexagonus* for ODP Sites 1239 and 1240, respectively (Fig. 4; Rincón-Martínez et al., 2010; Rippert et al., 2017).

The rhyolitic ash layer lies between 6.72 and 6.88 mcd in ODP Site 1239C. This stratigraphic position corresponds to a cooling event that occurred during the interglacial marine isotope stage 7d (sensu Railsback et al., 2015; Fig. 4), as pointed out by both alkenone temperature estimate and increase of benthic $\delta^{18}O$ values (Rincón-Martínez et al., 2010; red curve, Fig. 4). Based on the ODP Site 1239 age model (Rincón-Martínez et al., 2010), this tephra is dated at ~ 225 ka. Similarly, in the most distal ODP Site 1240, the rhyolitic ash layer lies between 25.69 to 25.72 mcd. It is in an equivalent stratigraphic position than in ODP Site 1239, as indicated by the $\delta^{18}O$ record performed on planktonic foraminifera (Rippert et al., 2017; Fig. 4), and the isotopic stage 7d cooling event inferred by sea-surface temperature reconstructions (Pena et al., 2008).

Bowles et al. (1973), and Ninkovich and Shackleton (1975), identified a similar rhyolitic ash layer, the "Layer L", off the coast of Colombia, Ecuador and northern Peru. Ninkovich and Shackleton (1975) suggested that the volcanic source is located in southern Colombia or Ecuador, based on the thickness of the deposits and the chemical composition of glass shards. The $\delta^{18}O$ records on the benthic foraminifera *Uvigerina proboscidea* within V19-28 and V19-29 cores (Fig. 1A) show that the volcanic event associated with the

"Layer L" occurred during the first cooling episode of the interglacial marine stage 7 (Ninkovich and Shackleton, 1975).

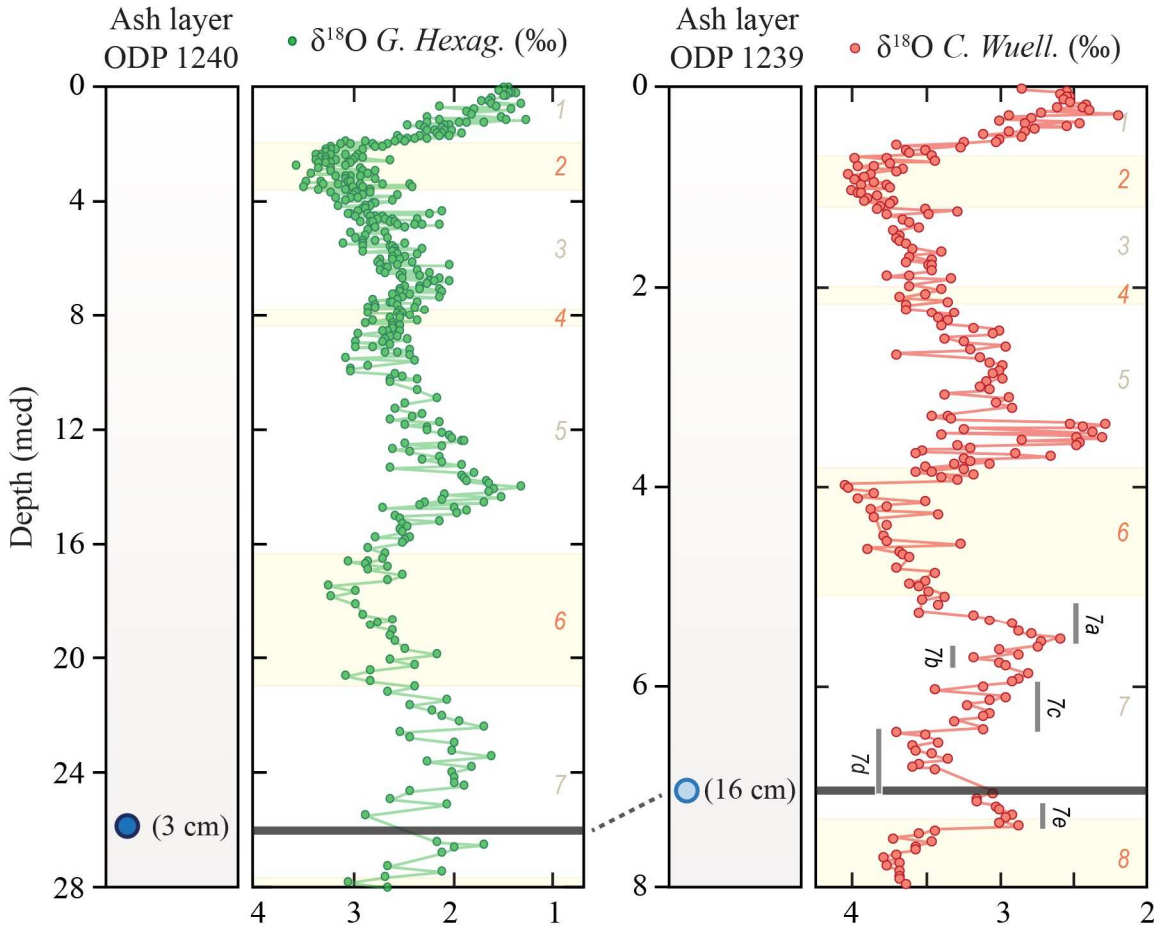

Fig. 4. $\delta^{18}O$ (‰) record of the planktonic *Globorotaloides hexagonus* (green curve; modified from Rippert et al., 2017) and benthic *Cibicidoides wuellerstorfi* (red curve, modified from Rincón-Martínez et al., 2010) foraminifera as a function of depth, for the ODP Sites 1240 and 1239 (Hole C), respectively. Depth of the ash layer presented in this study are represented by circles (symbols as in Fig. 3), and its thickness is indicated in parentheses. White and yellow fields represent marine isotope stages (MIS) defined by Lisiecki and Raymo (2005). Substages of MIS 7 from Railsback et al. (2015).

Marine tephra and the Chalupas ignimbrite present homogeneous contents for all major elements, with similar MgO/Fe_2O_3 and CaO/K_2O ratios (Figs. 3A, B and C). Marine tephra are slightly more enriched in SiO_2 and present a larger K_2O range than continental ignimbrite deposits (Fig. 3B). The whole-rock sample of the Chalupas ignimbrite is composed of a mixture of glass and crystals, whereas single shard measurements of marine tephra were performed on pristine glass, which concentrates incompatible elements and is slightly more

differentiated. Another hypothesis is that marine tephra might originate from a major explosion that occurred in early eruptive phase of the event, while continental ignimbrite deposits might have been emplaced latter, when the magma reservoir was emptying, emitting slightly less differentiated and more homogeneous magma. In addition, because the marine tephra layer off the Ecuadorian coast is significantly thicker than in the distal cores (Ninkovich and Shackleton, 1975; Shipboard Scientific Party, 2003), and based on its trace element signature that is typical of arc magmas (light and dark blue fields; Fig. 3D), it cannot originate from the Galápagos Islands (brown stars; Fig. 3A).

Considering the good match between the major element composition of marine tephra, and continental pumice samples combined to our new age determination, we can consider that the "Layer L" (Ninkovich and Shackleton, 1975), the ~6.8 m-deep ash layer in ODP Site 1239 (Fig. 4), the ~25.7 m-deep ash layer in ODP Site 1240, and the continental Chalupas ignimbrite deposit (sample 16EQ01) are related to the same ~216 ka Chalupas eruption.

It should be emphasized that the K-Ar age that we obtain for the Chalupas ignimbrite (216 ± 5 ka; Table 1) is slightly younger than that inferred from age models of deep-sea cores (~ 225 ka), although these ages are in agreement within 2-sigma uncertainty. Age models in ODP Sites 1239 and 1340 have been reconstructed using the global orbitally-tuned $\delta^{18}O$ benthic stack of Lisiecki and Raymo (2005), based on 57 worldwide cores, and with an average uncertainty of ~ 4 ka for the last million years (Lisiecki and Raymo, 2005). It is worth mentioning that benthic $\delta^{18}O$ records are related to sea-level changes, and that the $\delta^{18}O$ stack of Lisiecki and Raymo (2005) is essentially based on this signal. However, Skinner and Shackleton (2005) state that during the main climatic transitions, local changes in deep-water hydrography could account for a lag deep-eastern Pacific temperatures of ~ 4 ka when compared to the North Atlantic ones. Such further uncertainties should therefore be taken into account for age model reconstructions in this area. Hence, our new K-Ar age combined to $\delta^{18}O$ records offers a great potential to consider the Chalupas tephra as a new

chronostratigraphic marker for the marine isotopic stage 7 in the East Equatorial Pacific Ocean.

6.3. K-Ar dating of marine glass shards

In order to compare the age of both Chalupas continental ignimbrite and marine co-ignimbrite, we tentatively performed K-Ar dating on glass shards from the ODP 1239C core (section 1H5, intervals 43-45 and 38-40 cm), following the same sample preparation as for 16EQ01 (see Methods). Although the K content of both marine deposits is about 3.5%, in agreement with measurements performed on continental deposits (16EQ01; Table 1), the K-Ar ages we obtained for both marine deposits are meaningless, with values older than 700 ka for both of them. There is therefore probably a high radiogenic ^{40}Ar content in excess. It should be emphasized that deep-sea tephra are distal deposits made of thin particles that cooled rapidly during eruption. On the other hand, pumices within the massive (>50 m) proximal ignimbrite deposit probably cooled much slower, thereby allowing equilibrium with atmosphere. Consequently, any initial excess ^{40}Ar would have been removed from 16EQ01 ignimbrite glass, while it was trapped within the glass of distal tephra. Further analyses are required to investigate this important issue regarding the wider applicability of our dating technique.

6.4. Spatial distribution and volume of Chalupas eruption

There are no clear Plinian fall deposits associated with the 216 ± 5 ka Chalupas ignimbrite, but the offshore ash fall layer preserved in deep-sea cores (Ninkovich and Shackleton, 1975; Shipboard Scientific Party, 2003) and correlated in this study to that eruption (Figs. 3 and 4) seemingly corresponds to a co-ignimbrite ash deposit that shows a consistent thinning pattern from a source in sub-central Ecuador at Chalupas caldera.

Although offshore thickness could have been biased by ocean currents, slumping or bioturbation (Manville and Wilson, 2004; Wetzel, 2009; Lowe, 2011), the ash layer thickness data allowed us designing a tentative isopach map with 1, 7 and 15 cm contour lines (areas of ~1.6x10^6 km², 5.4x10^5 km² and 1.7x10^5 km², respectively; Fig. 5A) in order to derive a plot of ash thickness decay rate (i.e. thickness against square root of isopach area). Because we have only three contour lines, we calculated the minimal ash volume using the single isopach approach of Legros (2000), which yields bulk co-ignimbrite ash volumes in the range of about 60 to 140 km^3, with an average close to 100 km^3. A more realistic approximation that assumes an exponential thickness decay rate from the source and a fit to our data (using two or three isopachs on a single exponential segment, Pyle, 1989) yields volumes in the range of about 120 to 155 km^3, values that are considered reliable based on our data set.

The bulk volume of the continental ignimbrite around the caldera and in the Interandean Valley (beige field, total area of ~3150 km²; Fig. 5B) was estimated on a gross scale through delineating the envelope of known outcrops (red triangles; Beate et al., 2006; Bernard et al., 2008; Bustillos, 2008; Hall and Mothes, 2008a, 2008b; Ordóñez, 2012; Córdova, 2018; Jackson et al., 2019; this study; Fig. 5B), extrapolating the distribution of the ignimbrite in nearby valleys, and assuming from literature data and our field observations an average thickness of about 25-35 m. Results point to a bulk ignimbrite volume in the range of 80 to 110 km^3 (95 ± 15 km^3), slightly above previous literature estimates of 80-200 km^3 (Beate et al., 2006; Hall and Mothes, 2008a).

The total bulk deposit volume of both ignimbrite and co-ignimbrite thus amounts to about 200-265 km^3 (~230 ± 30 km^3). This result ranks the 216 ± 5 ka Chalupas eruption at VEI 7, consistent with the associated ~16 x 18 km caldera size (Lipman, 1999; Geshi et al., 2014). As a comparison, the volume erupted at Chalupas caldera is about two times larger than volumes released by historic eruptions of Tambora, Samalas, Krakatoa and Santorini (e.g., Lipman, 1999; Self et al., 2004; Lavigne et al., 2013; Karátson et al., 2018). Therefore,

the Chalupas event may be the largest Quaternary eruption from the Northern Andean Volcanic Zone and it can be envisioned that such an eruption could have caused a short-term climate forcing, with a possible global cooling. Measurements of sulphide contents contained in fluid inclusions of the glass shards are needed to quantify the amount of volatiles injected into the atmosphere, and to better infer the climatic impact of this super-eruption.

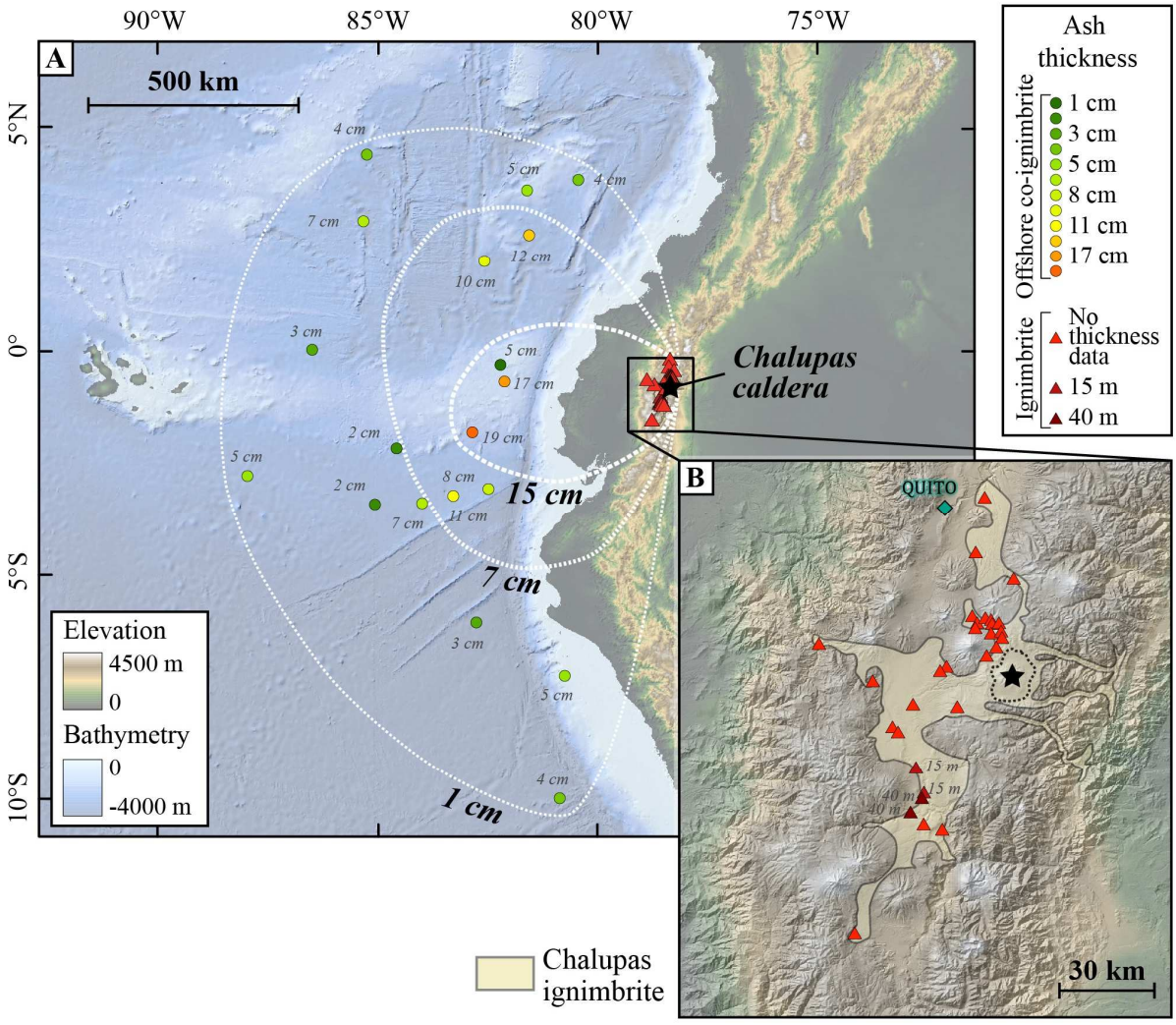

Fig. 5. A) Tentative isopach map (1, 7 and 15 cm) of the 216 ± 5 ka Chalupas offshore co-ignimbrite ash fall deposit. Location of the cores shown as orange, yellow and green circles and thickness data are from Ninkovich and Shackleton (1975) and Shipboard Scientific Party (2003). B) Reconstructed distribution of the Chalupas ignimbrite (beige field). Location of selected exposure sites shown as red triangles and ignimbrite thickness values are from Beate et al. (2006); Bernard et al. (2008); Bustillos (2008); Hall and Mothes (2008a; 2008b); Ordóñez (2012); Córdova (2018); Jackson et al. (2019); and this study. The Chalupas caldera is shown with a solid star, and its rim is depicted with a dotted line.

7. Conclusions

The present study demonstrates the reliability of the K-Ar dating method performed on glass shards from a massive continental ignimbrite deposit. This method is a reliable tool to date Quaternary pyroclastic deposits. The samples require a careful selection of only very fresh material, and removal of all altered and/or vesiculated glass shards. We provide a new K-Ar age of 216 ± 5 ka for the Chalupas ignimbrite.

Based on glass shard morphology, whole-rock and glass geochemical data, as well as isopach map of deposits, we have correlated the Chalupas ignimbrite to marine ash-layers from several cores offshore Ecuador. It shows that the Chalupas eruption could have injected between 200 and 265 km^3 of pyroclastic material into the atmosphere, and that ashes have reached areas located more than 900 km away from the source caldera.

Our K-Ar age obtained for Chalupas ignimbrite also provides reliable independent timing control for the $\delta^{18}O$ records of isotope stage 7, which is tuned by orbitally derived times-scales.

Finally, we hope that our study will reinforce the interest of jointly studying continental volcanic deposits and marine tephra layers to better characterize the major Pleistocene eruptions of the Ecuadorian arc. Such an approach also appears to be the only way to identify catastrophic eruptions that occurred during early stages of the current Ecuadorian arc construction, and could help to better define the recurrence of such major events.

Acknowledgments

The authors are grateful to Roelant van der Lelij and to an anonymous reviewer for their detailed reviews, constructive comments and suggestions, which contributed to improve this manuscript. The authors also wish to thank the Instituto Geofísico of Quito (IG-EPN) for their support during field

work. We are grateful to Amaëlle Landais and Rita Traversi for their help and advice concerning ice core data, as well as the Chalupas quarry manager who gave us permission to sample. Special thanks to the International Ocean Discovery Program (IODP) for providing us with the core samples, and Guillaume Leduc for details regarding $\delta^{18}O$ data obtained at ODP 1239 Site. This work is part of the Laboratoire Mixte International "Séismes et Volcans dans les Andes du Nord" program, an Ecuadorian-French cooperation program between the IG-EPN and the French Institut de Recherche pour le Développement (IRD). Field work and analyses were supported by INSU CNRS TelluS Aleas ([INSU 2015-ALEAS], [INSU 2016-ALEAS]) and LMI IRD ([2012-16 LMI SVAN-IRD]) programs. This is LGMT contribution number XXX and Laboratory of Excellence ClerVolc contribution number XXX.

References cited

Alvarado, A., Audin, L., Nocquet, J.M., Lagreulet, S., Segovia, M., Font, Y., Lamarque, G., Yepes, H., Mothes, P., Rolandone, F., Jarrín, P., Quidelleur, X., 2014. Active tectonics in Quito, Ecuador, assessed by geomorphological studies, GPS data, and crustal seismicity. Tectonics. 33, 67–83. http://doi.org/10.1002/2012TC003224.

Ancellin, M.-A., Samaniego, P., Vlastélic, I., Nauret, F., Gannoun, A., Hidalgo, S., 2017. Across-arc versus along-arc Sr-Nd-Pb isotope variations in the Ecuadorian volcanic arc. Geochemistry, Geophysics, Geosystems. 18, 1163–1188. http://doi.org/10.1002/2016GC006679.

Bablon, M., Quidelleur, X., Samaniego, P., Le Pennec, J.-L., Lahitte, P., Liorzou, C., Bustillos, J.E., Hidalgo, S., 2018. Eruptive chronology of Tungurahua volcano (Ecuador) revisited based on new K-Ar ages and geomorphological reconstructions, Journal of Volcanology and Geothermal Research. 357, 378–398. http://doi.org/10.1016/j.jvolgeores.2018.05.007.

Bablon, M., Quidelleur, X., Samaniego, P., Le Pennec, J.-L., Audin, L. Jomard, H., Baize, S., Liorzou, C., Hidalgo, S., Alvarado, A., 2019a. Interactions between volcanism and geodynamics in the southern termination of the Ecuadorian arc. Tectonophysics. 751, 54–14. http://doi.org/10.1016/j.tecto.2018.12.010.

Bablon, M., Quidelleur, X., Samaniego, P., Le Pennec, J.-L., Santamaria, S., Liorzou, C., Hidalgo, S., Eschbach, B., 2019b. Volcanic history reconstruction in northern Ecuador: insights for eruptive and erosion rates on the whole Ecuadorian arc. Bulletin of Volcanology, submitted.

Barberi, F., Coltelli, M., Ferrara, G., Innocenti, F., Navarro, J.M., Santacroce, R., 1988. Plio-Quaternary Volcanism in Ecuador. Geochemical Magazine. 125, 1–14.

Beate, B., Hammersley, L., DePaolo, D., and Deino, A.I., 2006, La Edad de la Ignimbrita de Chalupas, prov. de Cotopaxi, Ecuador, y su importancia como marcador estratigráfico. 6th Jornadas en Ciencias de la Tierra (EPN, Quito), Abstract book, 68–71.

Béguelin, P., Chiaradia, M., Beate, B., Spikings, R., 2015. The Yanaurcu volcano (Western Cordillera, Ecuador): A field, petrographic, geochemical, isotopic and geochronological study. Lithos. 218-219, 37–53. http://doi.org/10.1016/j.lithos.2015.01.014.

Bernard, B., van Wyk de Vries, B., Barba, D., Leyrit, H., Robin, C., Alcaraz, S., Samaniego, P., 2008. The Chimborazo sector collapse and debris avalanche: Deposit characteristics as evidence of emplacement mechanisms. Journal of Volcanology and Geothermal Research. 176, 36–43. http://doi.org/10.1016/j.jvolgeores.2008.03.012.

Bernard, B., Andrade, D., 2011. Volcanes Cuaternarios del Ecuador Continental. Map 1:500000.

Bernard, J., Kelfoun, K., Le Pennec, J.-L., and Vallejo Vargas, S., 2014. Pyroclastic flow erosion and bulking processes: comparing field-based vs. modeling results at Tungurahua volcano, Ecuador. Bulletin of Volcanology, 76. http://doi.org/10.1007/s00445-014-0858-y.

Bigazzi, G., Coltelli, M., Hadler, N.J.C., Araya, A.M.O., Oddone, M., Salazar, E., 1992. Obsidian-bearing lava flows and pre-Columbian artifacts from the Ecuadorian Andes: First new multidisciplinary data. Journal of South American Earth Science. 6, 21–32. http://doi.org/10.1016/0895-9811(92)90014-P.

Bowles, F.A., Jack, R.N., Carmichael, I.S.E., 1973. Investigation of deep-sea volcanic ash layers from equatorial Pacific cores. Geological Society of America Bulletin. 84, 2371–2388.

Bryant, J.A., Yogodzinski, G.M., Hall, M.L., Lewicki, J.L., Bailey, D.G., 2006. Geochemical Constraints on the Origin of Volcanic Rocks from the Andean Northern Volcanic Zone, Ecuador. Journal of Petrology. 47, 1147–1175. http://doi.org/10.1093/petrology/egl006.

Bustillos, J.E., 2008. Las avalanchas de escombros en el sector del volcan Tungurahua. Facultad de ingenieria en geologia y petroleos, Escuela Politecnica Nacional, Quito.

Carey, S., 1997. Influence of convective sedimentation on the formation of widespread tephra fall layers in the deep sea. Geology. 25(9), 839–842. https://doi.org/10.1130/0091-7613(1997)025<0839:IOCSOT>2.3.CO.

Cerling, T.E., Brown, F.H., Bowman, J.R., 1985. Low-temperature alteration of volcanic glass: hydration, Na, K, ^{18}O and Ar mobility. Chemical Geology, Isotope Geoscience Section. 52, 281–293.

Chiaradia, M., Barnes, J.D., Cadet-Voisin, S., 2014. Chlorine stable isotope variations across the Quaternary volcanic arc of Ecuador. Earth and Planetary Science Letters. 396, 22–33. http://doi.org/10.1016/j.epsl.2014.03.062.

Cole-Dai, J., 2010. Volcanoes and climate. Wiley Interdisciplinary Reviews: Climate Change. 1, 824–839, http://doi.org/10.1002/wcc.76.

Córdova, M., 2018. Identificación y caracterización de los últimos productos eruptivos de la fase resurgente de la caldera de Chalupas. Escuela Politécnica Nacional, Quito, 133.

Córdova, M., Mothes, P., Hall, M., Telenchana, E., 2018. Identification and characterization of the youngest eruptive products of the Chalupas Caldera, Ecuador: An update on the caldera. Cities on Volcanoes 10, Abstract ID: 438.

Cotten, J., Le Dez, A., Bau, M., Caroff, M., Maury, R.C., Dulski, P., Fourcade, S., Bohn, M., Brousse, R., 1995. Origin of anomalous rare-earth element and yttrium enrichments in subaerially exposed basalts: Evidence from French Polynesia. Chemical Geology. 119, 115–138.

Dyez, K.A., Ravelo, A.C., Mix, A.C., 2016. Evaluating drivers of Pleistocene eastern tropical Pacific sea surface temperature. Paleoceanography. 31, 1054–1069. http://doi.org/10.1002/2015PA002873.

Ellis, B.S., Mark, D.F., Pritchard, C.J., Wolff, J.A., 2012. Temporal dissection of the Huckleberry Ridge Tuff using the $^{40}Ar/^{39}Ar$ dating technique. Quaternary Geochronology. 9, 34–41. https://doi.org/10.1016/j.quageo.2012.01.006.

Espín, P.A., 2014. Caracterización geológica y litológica de los depósitos laháricos de Mera, provincia de Pastaza. Ph.D. tesis, Facultad de Geología y Petróleos, EPN, Quito, 213 p.

Garrison, J.M., Davidson, J.P., Hall, M., Mothes, P., 2011. Geochemistry and Petrology of the Most Recent Deposits from Cotopaxi Volcano, Northern Volcanic Zone, Ecuador. Journal of Petrology. 52, 1641–1678. https://doi.org/10.1093/petrology/egr023.

Germa, A., Quidelleur, X., Gillot, P.Y., Tchilinguirian, P., 2010. Volcanic evolution of the back-arc Pleistocene Payun Matru volcanic field (Argentina). Journal of South American Earth Sciences. 29, 717–730. https://doi.org/10.1016/j.jsames.2010.01.002.

Germa, A., Quidelleur, X., Lahitte, P., Labanieh, S., Chauvel, C., 2011. The K-Ar Cassignol–Gillot technique applied to western Martinique lavas: A record of Lesser Antilles arc activity from 2 Ma to Mount Pelée volcanism. Quaternary Geochronology. 6, 341–355, https://doi.org/10.1016/j.quageo.2011.02.001.

Geshi, N., Rush, J., Acocella, V., 2014. Evaluating volumes for magma chambers and magma withdrawn for caldera collapse. Earth and Planetary Science Letters. 396, 107–115, https:// https://doi.org/10.1016/j.epsl.2014.03.059.

Gillot, P.-Y., Hildenbrand, A., Lefèvre, J.-C., Albore-Livadie, C., 2006. The K/Ar dating method : principle, analytical techniques, and application to Holocene volcanic eruptions in Southern Italy. Acta Vulcanologica. 18, 55–66.

Hall, M.L., Mothes, P.A., 1997. Origin and age of the Upper Cangahua Formation, Tumbaco Valley (Ecuador). Suelos volcánicos endurecidos, Mem. III Symp. Intern. ORSTOM (EPN, Quito, dec. 1996), 19–28.

Hall, M., Mothes, P., 2008a. The rhyolitic–andesitic eruptive history of Cotopaxi volcano, Ecuador. Bulletin of Volcanology. 70, 675–702. https://doi.org/10.1007/s00445-007-0161-2.

Hall, M., Mothes, P., 2008b, Quilotoa volcano - Ecuador: An overview of young dacitic volcanism in a lake-filled caldera: Journal of Volcanology and Geothermal Research, v. 176, p. 44–55, doi: 10.1016/j.jvolgeores.2008.01.025.

Hall, M., Mothes, P., 2008c. The Chacana caldera complex in Ecuador. IOP Conference Series: Earth and Environmental Science. 3, https://doi.org/10.1088/1755-1307/3/1012004.

Hammersley, L., 2003. The Chalupas Caldera. Ph.D. thesis, Berkeley, University of California, 201 p.

Hess, J.C., Lippolt, H.J., 1994. Compilation of K-Ar measurements on HD-B1 standard biotite. 1994 status report, Phanerozoic time Scale. Bull. Liais. Inform. IUGS Subcomm. Geochronol., 122.

Hora, J.M., Singer, B.S., Jicha, B.R., Beard, B.L., Johnson, C.M., de Silva, S., Salisbury, M., 2010. Volcanic biotite-sanidine $^{40}Ar/^{39}Ar$ age discordances reflect Ar partitioning and pre-eruption closure in biotite. Geology. 38, 923–926.

Jackson, L.J., Horton, B.K., Beate, B.O., Bright, J., Breecker, D.O., 2019. Testing stable isotope paleoaltimetry with Quaternary volcanic glasses from the Ecuadorian Andes. Geology. 47, 411-414. https://doi.org/10.1130/G45861.1.

Karátson, D., Gertisser, R., Telbisz, T., Vereb, V., Quidelleur, X., Druitt, T., Nomikou, P., Kósik, S., 2018. Towards reconstruction of the lost Late Bronze Age intra-caldera island of Santorini, Greece. Scientific Reports. 8. https://doi.org/10.1038/s41598-018-25301-2.

Lacasse, C., van den Bogaard, P., 2002. Enhanced airborne dispersal of silicic tephras during the onset of Northern Hemisphere glaciations, from 6 to 0 Ma records of explosive volcanism and climate change in the subpolar North Atlantic. Geology. 30, 623–626.

Lavigne, F., Degeai, J.-P., Komorowski, J.-C., Guillet, S., Robert, V., Lahitte, P., Oppenheimer, C., Stoffel, M., Vidal, C.M., Surono, Pratomo, I., Wassmer, P., Hajdas, I., Hadmoko, D.S., de Belizal, E., 2013. Source of the great A.D. 1257 mystery eruption unveiled, Samalas volcano, Rinjani Volcanic Complex, Indonesia. Proceedings of the National Academy of Sciences. 110, 16742–16747. https://doi.org/10.1073/pnas.1307520110.

Legros, F., 2000. Minimum volume of a tephra fallout deposits estimated from a single isopach. Journal of Volcanology and Geothermal Research. 96 (1-2), 25-32. https://doi.org/10.1016/S0377-0273(99)00135-3

Lipman, P, 1999. Caldera, Haraldur Sigurdsson, ed. Encyclopedia of Volcanoes. ISBN 0-12-643140-X.

Lisiecki, L.E., Raymo, M.E., 2005. A Pliocene-Pleistocene stack of 57 globally distributed benthic δ18O records. Paleoceanography, 20. https://doi.org/10.1029/2004PA001071.

Lowe, D.J., 2011. Tephrochronology and its application: A review. Quaternary Geochronology. 6, 107–153. https://doi.org/10.1016/j.quageo.2010.08.003.

Manville, V., Wilson, C.J.N., 2004. Vertical density currents: a review of their potential role in the deposition and interpretation of deep-sea ash layers. Journal of the Geological Society. 161, 47-958.

Mark, D.F., Petraglia, M., Smith, V.C., Morgan, L.E., Barfod, D.N., Ellis, B.S., Pearce, N.J., Pal, J.N., Korisettar, R., 2014. A high-precision $^{40}Ar/^{39}Ar$ age for the Young Toba Tuff and dating of ultra-distal tephra: Forcing of Quaternary climate and implications for hominin occupation of India. Quaternary Geochronology. 21, 90–103. https://doi.org/10.1016/j.quageo.2012.12.004.

Matthews, N.E., Vazquez, J.A., Calvert, A.T., 2015. Age of the Lava Creek supereruption and magma chamber assembly at Yellowstone based on $^{40}Ar/^{39}Ar$ and U-Pb dating of sanidine and zircon crystals. Geochemistry, Geophysics, Geosystems. 16, 2508–2528. https://doi.org/10.1002/2015GC005881.

McCormick, P., Thomason, L.W., Trepte, C.R., 1995. Atmospheric effects of the Mt Pinatubo. Nature. 373, 399–404.

McDougall, I., Harrison, T.M., 1999. Geochronology and thermochronology by the $^{40}Ar/^{39}Ar$ method, second ed. United States, Oxford University Press.

Mills, M.J., 2000. Volcanic aerosol and global atmospheric effects, Haraldur Sigurdsson, ed. Encyclopedia of Volcanoes. ISBN 0-12-643140-X.

Milne, J.D.G., 1973. Mount Curl Tephra, a 230000-year-old implications for Quaternary chronology marker bed in New Zealand, and its. New Zealand Journal of Geology and Geophysics. 16, 519–532. https://doi.org/10.1080/00288306.1973.10431375.

Monzier, M., Robin, C., Samaniego, P., Hall, M.L., Cotten, J., Mothes, P., Arnaud, N., 1999. Sangay volcano, Ecuador: structural development, present activity and petrology. Journal of Volcanology and Geothermal Research. 90, 49–79.

Morgan, L.E., Renne, P.R., Taylor, R.E., WoldeGabriel, G., 2009. Archaeological age constraints from extrusion ages of obsidian: Examples from the Middle Awash, Ethiopia. Quaternary Geochronology. 4, 193–203, https://doi.org/10.1016/j.quageo.2009.01.001.

Mothes, P, Hall, M.L., 2008. Rhyolitic calderas and centers clustered within the active andesitic belt of Ecuador's Eastern Cordillera. IOP Conference Series: Earth and Environmental Science. 3, https://doi.org/10.1088/1755-1307/3/1/012007.

Ninkovich, D., Shackleton, N.J., 1975. Distribution, stratigraphic position and age of ash layer “L”, in the Panama Basin region. Earth and Planetary Science Letters. 27, 20–34.

Ordóñez, J., 2012. Depósitos volcánicos del Pleistoceno Tardío en la cuenca de. Ambato: caracterización, distribución y origen. Ph.D. tesis, Facultad de Geología y Petróleos (Quito, EPN), 213 p.

Pinti, D.L., Quidelleur, X., Chiesa, S., Ravazzi, C., Gillot, P.-Y., 2001. K-Ar dating of an early Middle Pleistocene distal tephra in the interglacial varved succession of Pianico-Sellere (Southern Alps, Italy). Earth and Planetary Science Letters, 188, 1–7.

Pena, L. D., Cacho, I., Ferretti, P., Hall, M. A., 2008. El Niño–Southern Oscillation-like variability during glacial terminations and interlatitudinal teleconnections. Paleoceanography. 23, PA3101. https://doi.org/10.1029/2008PA001620.

Pyle, D.M., 1989. The thickness, volume and grainsize of tephra fall deposits. Bulletin of Volcanology. 51 (1), 1-15.

Railsback, L.B., Gibbard, P.L., Head, M.J., Voarintsoa, N.R.G., Toucanne, S., 2015. An optimized scheme of lettered marine isotope substages for the last 1.0 million years, and the climatostratigraphic nature of isotope stages and substages. Quaternary Science Reviews. 111, 94–106. https://doi.org/10.1016/j.quascirev.2015.01.012.

Ricci, J., Quidelleur, X., Lahitte, P., 2015. Volcanic evolution of central Basse-Terre Island revisited on the basis of new geochronology and geomorphology data. Bulletin of Volcanology. 77, https://doi.org/10.1007/s00445-015-0970-7.

Rincón-Martínez, D., Lamy, F., Contreras, S., Leduc, G., Bard, E., Saukel, C., Blanz, T., Mackensen, A., Tiedemann, R., 2010. More humid interglacials in Ecuador during the past 500 kyr linked to latitudinal shifts of the equatorial front and the Intertropical Convergence Zone in the eastern tropical Pacific. Paleoceanography. 25, PA2210. https://doi.org/10.1029/2009PA001868.

Robin, C., Eissen, J.-P., Samaniego, P., Martin, H., Hall, M., Cotten, J., 2009. Evolution of the late Pleistocene Mojanda–Fuya Fuya volcanic complex (Ecuador), by progressive adakitic involvement in mantle magma sources. Bulletin of Volcanology. 71, 233–258. https://doi.org/10.1007/s00445-008-0219-9.

Robock, A., 2000. Volcanic Eruptions and Climate. Reviews of Geophysics. 38, 191–219.

Rose, W.I., Durant, A.J., 2009. Fine ash content of explosive eruptions. Journal of Volcanology and Geothermal Research. 186, 32–39. https://doi.org/10.1016/j.jvolgeores.2009.01.010.

Rippert, N., Max, L., Mackensen, A., Cacho, I., Povea, P., Tiedemann, R., 2017. Alternating Influence of Northern Versus Southern-Sourced Water Masses on the Equatorial Pacific Subthermocline During the Past 240 ka. Paleoceanography. 32, 1256–1274. https://doi.org/10.1002/2017PA003133.

Samaniego, P., Martin, H., Monzier, M., Robin, C., Fornari, M., Eissen, J.-P., Cotten, J., 2005. Temporal Evolution of Magmatism in the Northern Volcanic Zone of the Andes: The Geology and Petrology of Cayambe Volcanic Complex (Ecuador). Journal of Petrology. 46, 2225–2252. https://doi.org/10.1093/petrology/egi053.

Samaniego, P., Barba, D., Robin, C., Fornari, M., and Bernard, B., 2012. Eruptive history of Chimborazo volcano (Ecuador): A large, ice-capped and hazardous compound volcano in the Northern Andes. Journal of Volcanology and Geothermal Research. 221–222, 33–51, https://doi.org/10.1016/j.jvolgeores.2012.01.014.

Samper, A., Quidelleur, X., Komorowski, J.-C., Lahitte, P., Boudon, G., 2009. Effusive history of the Grande Découverte Volcanic Complex, southern Basse-Terre (Guadeloupe, French West Indies) from new K-Ar Cassignol–Gillot ages. Journal of Volcanology and Geothermal Research. 187, 117–130, https://doi.org/10.1016/j.jvolgeores.2009.08.016.

Schindlbeck, J.C., Kutterolf, S., Freundt, A., Alvarado, G.E., Wang, K.-L., Straub, S.M., Hemming, S.R., Frische, M., Woodhead, J.D., 2016a. Late Cenozoic tephrostratigraphy offshore the southern Central American Volcanic Arc: 1. Tephra ages and provenance. Geochemistry, Geophysics, Geosystems, 17, 4641–4668. https://doi.org/10.1002/2016GC006503.

Schindlbeck, J.C., Kutterolf, S., Freundt, A., Straub, S.M., Vannucchi, P., Alvarado, G.E., 2016b. Late Cenozoic tephrostratigraphy offshore the southern Central American Volcanic Arc: 2. Implications for magma production rates and subduction erosion. Geochemistry, Geophysics, Geosystems. 17, 4585–4604. https://doi.org/10.1002/2016GC006504.

Self, S., Gertisser, R., Thordarson, T., Rampino, M.R., Wolff, J.A., 2004. Magma volume, volatile emissions, and stratospheric aerosols from the 1815 eruption of Tambora. Geophysical Research Letters. 31, 1–4. https://doi.org/10.1029/2004GL020925.

Shipboard Scientific Party, 2003. Sites 1238, 1239 and 1240, Mix, A.C., Tiedemann, R., Blum, P., et al., Proceedings of Ocean Drill Program, Initial Report, 202.

Skinner, L.C., Shackleton, N.J., 2005. An Atlantic lead over Pacific deep-water change across Termination I: implications for the application of the marine isotope stage stratigraphy. Quaternary Science Reviews. 24, 571–580. https://doi.org/10.1016/j.quascirev.2004.11.008.

Steiger, R.H., Jäger, E., 1977. Subcommission on geochronology: convention on the use of decay constants in geo- and cosmochronology. Earth and Planetary Science Letters. 36, 359–362.

Wiesner, M.G., Wang, Y., Zheng L., 1995. Fallout of volcanic ash to the deep South China Sea induced by the 1991 eruption of Mount Pinatubo. Geology. 23, 885–888.

Storey, M., Roberts, R.G., Saidin, M., 2012. Astronomically calibrated $^{40}Ar/^{39}Ar$ age for the Toba supereruption and global synchronization of late Quaternary records. Proceedings of the National Academy of Sciences. 109, 18684–18688. https://doi.org/10.1073/pnas.1208178109.

Sun, S.-s., McDonough, W.F., 1989. Chemical and isotopic systematics of oceanic basalts: implications for mantle composition and processes. Geol. Soc. Lond. Spec. Publ. 42, 313–345. https://doi.org/10.1144/GSL.SP.1989.042.01.19.

Wetzel, A., 2009. The preservation potential of ash layers in the deep-sea: the example of the 1991-Pinatubo ash in the South China Sea. Sedimentology. 56, 1992-2009.

Williams, M.A.J., Ambrose, S.H., van der Kaars, S., Ruehlemann, C., Chattopadhyaya, U., Pal, J., Chauhan, P.R., 2009. Environmental impact of the 73ka Toba super-eruption in South Asia. Palaeogeography, Palaeoclimatology, Palaeoecology. 284, 295–314. https://doi.org/10.1016/j.palaeo.2009.10.009.

743

744 **Appendix A**
745 Whole-rock major and trace element composition of Chalupas ignimbrite samples (unpublished IRD-IG dataset),
746 measured by ICP-AES at the Laboratoire Géosciences Océan of the Université de Bretagne Occidentale (Brest,
747 France; Cotten et al., 1995). All analyses of major elements were brought down to a total of 100% on a water-
748 free basis. Outcrop coordinates projected using the Universal Transverse Mercator (UTM) coordinate system
749 (Zone 17) and given within 100 meters (Fig. 1).

750

		Whole-rock Chalupas ignimbrite													
		CHAL 00	CHAL 01 TAMBO	CHAL 01A	CHAL 02A TIS	CHAL 02C TIS	CHAL 02D TIS	CHAL 118	CHAL 750165	CHAL 862348-ING	CHAL 870588	CHAL 893794-AC	CHAL 933243-YPF	COT FD 183 F	CHAL RIO 23
	UTM E	798800	789800	778000	778000	754200	754200	754200	787000	775000	786200	787000	789300	793300	793300
	UTM S	9949300	9921400	9917500	9917500	9911200	9911200	9911200	9933000	9916500	9934800	9958800	9979400	9924300	9924300
Major elements (wt.%)	SiO_2	74.32	74.67	74.18	74.54	74.87	74.63	74.19	74.53	74.95	75.3	75.2	75.24	75.34	74.8
	TiO_2	0.26	0.27	0.26	0.24	0.25	0.24	0.26	0.26	0.24	0.24	0.24	0.24	0.24	0.24
	Al_2O_3	13.78	14.35	14.26	13.71	13.64	13.71	14.11	14.17	13.8	13.75	13.63	13.79	13.73	13.55
	Fe_2O_3	1.61	1.61	1.49	1.45	1.49	1.41	1.48	1.6	1.4	1.47	1.47	1.35	1.4	1.45
	CaO	1.32	1.28	1.2	1.16	1.2	1.14	1.23	1.28	1.29	1.23	1.23	1.18	1.17	1.46
	MgO	0.3	0.34	0.33	0.32	0.33	0.3	0.35	0.33	0.3	0.3	0.29	0.29	0.32	0.31
	MnO	0.04	0.05	0.05	0.05	0.05	0.05	0.05	0.05	0.05	0.05	0.05	0.05	0.05	0.04
	K_2O	4.46	4.18	4.23	4.72	4.52	4.66	4.54	4.26	4.29	4.19	4.13	4.34	4.28	4.39
	Na_2O	3.86	3.2	3.94	3.78	3.61	3.84	3.74	3.47	3.64	3.44	3.71	3.48	3.44	3.71
	P_2O_5	0.05	0.04	0.04	0.03	0.03	0.03	0.04	0.05	0.04	0.03	0.04	0.03	0.03	0.03
	L.O.I.	*3.68*	*5.41*	*3.16*	*2.95*	*2.69*	*3.4*	*2.88*	*5.19*	*3.38*	*3.15*	*4.21*	*3.96*	*5.37*	*3.77*
Trace elements (ppm)	Sc	2.1	2.1	1.8	2	2	2	1.9	2.2	2	2	2	1.9	2	1.8
	V	12	15	12	12	12	11	12.5	15	13	10	13	10	10	11
	Cr	3	5	3	2	2	2	5	4	4	3	2	2	2	3
	Co	1.5	5	1.5	9	5	4.5	1.5	2	1	2	3	2	2	2
	Ni	1.5	4	1	1	2	2	1	4	2	2	1	1.5	4	2
	Rb	174	178	170	170	168	170	177	167	174	181	178	165	167	167
	Sr	215	200	217	209	213	204	222	203	205	210	210	199	202	210
	Y	11.8	13	13.4	12.8	12.6	12.5	14	12.3	12.5	12.2	12.9	12	15	12.5
	Zr	145	155	155	162	162	152	153	149	154	160	170	156	164	160
	Nb	11	11	11.5	11.4	11.5	11.5	11.2	10.5	11.15	10.9	11.4	11	11.1	11.4
	Ba	1060	1010	1100	1080	1120	1080	1095	1005	1080	1000	1050	997	1140	1080
	La	32	31	32	31	31	31	32.5	30.75	32.5	30	31	29.5	31	31
	Ce	56	60	56	57	55	58	57	55	57	57	60	55	58	56
	Nd	21	23	20.5	20.5	21	21.5	21.5	21	21	20	20	20.4	21.5	23
	Sm	3.3		3.85	3.6	3.65	3.6	3.45			3.7	3.5		3.5	3.5
	Eu	0.67	0.55	0.68	0.58	0.58	0.6	0.66	0.58	0.6	0.58	0.56	0.57	0.62	0.56
	Gd	2.8		2.3	2.6	3.35	2.85	2.25			2.7	2.7		2.8	2.6
	Dy	1.9	2	2.28	2	2	2	2.2	2.1	2	2	2	1.9	2.3	1.95
	Er	1.2	1.3	1.3	1.2	1.25	1.2	1.4	1.2	1.3	1.2	1.25	1.25	1.4	1.2
	Yb	1.2	1.175	1.4	1.19	1.2	1.2	1.42	1.195	1.245	1.25	1.26	1.19	1.35	1.25
	Th	22.3		22	20	22.4	22.9	23.7			23.5	22.5	21.1	21.8	21

751